Nanoprobe Synthesized by Magnetotactic Bacteria, Detecting Fluorescence Variations under Dissociation of Rhodamine B from Magnetosomes following Temperature, pH Changes, or the Application of Radiation

Edouard Alphandéry, Darine Abi Haidar, Olivier Seksek, Maxime Thoreau, Alain Trautmann, Nadege Bercovici, Florence Gazeau, François Guyot, Imène Chebbi

A Nanoprobe Synthesized by Magnetotactic Bacteria, Detecting Fluorescence Variations under Dissociation of Rhodamine B from Magnetosomes following Temperature, pH Changes, or the Application of Radiations.

Edouard Alphandery[+,⊥,*], *Darine Abi-Haidar*[++,+++++], *Olivier Seksek*[++], *Maxime Thoreau*[+++], *Alain Trautmann*[+++], *Nadege Bercovici*[+++], *Florence Gazeau*[++++], *François Guyot*[+], *Imène Chebbi*[⊥]

[+]Institut de minéralogie, de physique des matériaux et de cosmochimie, UMR 7590 CNRS, Sorbonne Universités, UPMC, University Paris 06, Muséum National d'Histoire Naturelle, 4 Place Jussieu, 75005, Paris, France.

[⊥]Nanobacterie SARL, 36 boulevard Flandrin, 75116, Paris, France.

[++]Laboratoire d'imagerie et modélisation en neurobiologie et cancérologie, UMR 8165, Paris-Saclay University, Rue des Adèles, Campus d'Orsay Bâtiment 440, 91405, Orsay, France.

[+++]Institut Cochin, 22 rue Méchain, 75014, Paris, France.

[++++]Laboratoire de matière et systèmes complexes, MSC, Université Paris Diderot, bâtiment Condorcet, case 7056, 75205 Paris Cedex 13, France.

[+++++]Paris Diderot University, F-75013, Paris, France.

*Corresponding author Email address:

edouardalphandery@hotmail.com

KEYWORDS: magnetosomes, magnetotactic bacteria, fluorescent probe, thermometer, fluorescence, nanomedicine, magnetic hyperthermia, alternating magnetic field.

ABSTRACT: We report a method of fabrication of fluorescent magnetosomes, designated as MCR400, in which 400 µM of rhodamine B are introduced in the growth medium of AMB-1 magnetotactic bacteria and fluorescent magnetosomes are then extracted from these bacteria. These fluorescent magnetosomes behave differently from most fluorescent nanoprobes, which often lead to fluorescence losses over time due to photo-bleaching. Indeed, when MCR400 are heated to 30-90 °C, brought to an acidic pH, or exposed to radiations, we observed that their fluorescence intensity increased. We attributed this behavior to the dissociation of rhodamine B from the magnetosomes. Interestingly, enhanced fluorescence was also observed *in vitro* when MCR400 were mixed with either primary macrophages or tumor cells (TC1-GFP or RG2-Cells) or *in vivo* when MCR400 were introduced in rat glioblastoma. We showed that MCR400 internalize in tumor and immune cells (macrophages) leading to enhanced fluorescence, suggesting that fluorescent magnetosomes could be used during cancer treatments such as magnetic hyperthermia to image cells of interest such as immune or tumor cells.

1. INTRODUCTION

During the past few years, the design of nano-scale fluorescent probes has been considerably improved to yield a high level of sophistication[1]. With these probes, it is possible to detect locally a wide range of different parameters including intracellular pH[2], pH in solution[3,4], the presence of a cell membrane or organelles[5], molecules of interest, *e.g.* folic acid[6], the release of substances from nanoparticles, *e.g.* drugs such as doxorubicin[7], or toxic compounds such as mercury[8], temperature variations due for example to changes in intracellular Ca^{2+} concentration[9], or to the application of a radiation.[10] Detection can rely on the variation of the fluorescence intensity, wavelength[11], or lifetimes[7], with such parameter. These probes were made of various inorganic[3], organic[12,13] or biodegradable[14], nano-materials, in which fluorescent molecules could either be self-assembled into a nanomaterial[11], or bound, covalently or not, to existing nanoparticles[15]. They were either directly exposed to a potentially degrading surrounding environment or embedded in a protecting matrix, *e.g.* silica[15]. Nano-assembly could result in enhanced[16], or quenched[17,18,19] fluorescence. Mechanism responsible for the fluorescence properties of these probes was often reported to involve electron or energy transfer[20,21,22],, which is enhanced due to fluorescent molecules being in close proximity with each other or with nanoparticles. These probes were also functionalized to target specific cells, *e.g.* RGD peptides were conjugated to fluorescent nanoparticles to target $\alpha_v\beta_3$ integrin overexpressed in certain cancer cells[13]. Their design could yield fluorescence emission at several wavelengths[23], or combine fluorescence with other imaging methods, such as positron emission tomography[24]. In some cases, nanometric fluorescent probes were used for detection and treatment purposes, using for example photo-thermal therapy (PTT) or photodynamic therapy (PDT)[25]. Previous studies mainly reported the properties of chemically synthesized fluorescent nano-probes. However, it has been shown that a species of bacterium, called magnetotactic bacterium, synthetizes iron oxide nanoparticles called magnetosomes[26], with larger sizes, better crystallinity, and superior magnetic properties and heating power under the application of an alternating magnetic field compared with most chemically synthesized nanoparticles[27]. Due to these properties, magnetosomes were successfully tested for a wide range of different medical applications, including magnetic

hyperthermia and magnetic resonance imaging[28,29,30]. Fabrication of fluorescent magnetosomes were previously described, either involving genetic manipulations of magnetotactic bacteria to produce magnetosomes tagged with green fluorescent proteins[31,32], or a chemical hydrophobic interaction between a fluorophore (DiI) and magnetosomes extracted from magnetotactic bacteria[33]. However, genetic engineering could hardly yield a high magnetosome production yield, while fluorescent magnetosomes obtained by chemical adsorption were shown to image cells but not to detect other parameters[33].

In this study, we introduced a new method to synthesize fluorescent magnetosomes in which a solution of rhodamine B was introduced in the growth medium of magnetotactic bacteria in addition to the iron source[34]. Following their extraction from magnetotactic bacteria, magnetosomes appeared to be associated with rhodamine B. They were designated as MCR400. We compared the properties of MCR400 with those of two other types of magnetosomes in which we attempted to chemically associate rhodamine B to the magnetosomes either via a reaction between rhodamine B and magnetosomes (MC@RhB-1) or through direct adsorption of rhodamine B at magnetosome surface (MC@RhB-2). Absorption and fluorescent properties of the supernate of the suspensions containing MCR400, MC@RhB-1, and MC@RhB-2, obtained after magnetic separation, were studied to examine the presence (or not) of rhodamine B in the supernate and hence to deduce if rhodamine B has remained associated with the magnetosomes after magnetic separation. These properties were also studied when these suspensions were exposed to changes in temperature, pH or various levels of radiations. We examined if fluorescence changes were occurring to determine if the probe could be used to detect such parameters. Besides studies in solution, the fluorescent probe was also brought into contact with cells and administered inside the brain of rats to study fluorescent changes under these conditions and explore the use of this probe in an *in vitro* or *in vivo* environment.

2. EXPERIMENTAL SECTION

2.1. Synthesis of non-fluorescent chains of magnetosomes extracted from magnetotactic bacteria (MC). *Magnetospirillum magneticum* AMB-1 magnetotactic bacteria were obtained from

ATCC (ATCC 700274) and grown under microaerobic conditions at 30 °C in a growth medium slightly different from the MSGM medium (ATCC medium 1653). TEM images of whole magnetotactic bacteria, chains of magnetotosomes, and histograms of magnetosome sizes are presented in Fig. 1. In one litter, this medium contained 0.68 g of monobasic potassium phosphate, 0.85 g of sodium succinate, 0.57 g of sodium tartrate, 0.083 g of sodium acetate, 225 µl of 0.2% resazurin, 0.17 g of sodium nitrate, 0.04 g of L-ascorbic acid, 2 ml of a 10 mM iron quinate solution, 10 ml of a solution of Woolf vitamins and 5 ml of a solution of Woolf minerals. The pH of the culture medium was adjusted to 6.85 using a 1M sodium hydroxide solution. The bacteria were collected during the stationary phase and concentrated using a tangential flow filtration column (mPES, 500KDa) with a flow rate of 950 mL/min and then washed 5 times for 30 minutes with a solution of Phosphate buffer saline at pH 7.4 (137 mM NaCl, 2.7 mM KCl, 10 mM Na2HPO4, 1.76 mM KH2PO4). Bacteria were collected by centrifugation at 4000 rpm for 1 hour, the supernatant was removed and the bacteria were re-suspended in 50 mM Tris-HCl buffer solution at pH 7.4 and diluted to yield an optical density of 5 at 600 nm. To lyse cell membranes and extract magnetosomes from the bacteria, the bacterial suspension was sonicated at 30 W at 5 °C during 60 minutes with pulses of 2 sec. and an interval between pulses of 1 sec. Following sonication, magnetosome chains were magnetically isolated from cellular debris using a neodymium magnet. The supernatant containing the cellular debris was removed and magnetosome chains (MC) were washed five times magnetically with a 50 mM Tris-HCl buffer solution at pH 7.4 and then fifteen times with Millipore® water. They were finally re-suspended in Millipore® sterile water to obtain a suspension of MC.

2.2. Instrumentation. Electron transmission microscopy images of whole bacteria, MC@RhB-1, MC@RhB-2, and MCR400 were obtained with a JEM-2100 from JEOL. For that, 5 µl of a suspension of whole bacteria, MC@RhB-1, MC@RhB-2, and MCR400, were deposited on top of a carbon grid and dried. Size distributions of magnetosomes in MC@RhB-1, MC@RhB-2, and MCR400, were measured over 300 magnetosomes and plotted in histograms. For studies in solution, the absorption of the different suspensions was measured by a Varian Cary 3E UV-Vis spectrophotometer and the

fluorescence of these suspensions was detected using Aminco-Bowman 2 spectrofluorimeter (Edison, NJ). For imaging cells in the presence of MCR400, we either used an inverted microscope (TE2000-E; Nikon) equipped with a 20x objective, for optical imaging or a JEOL JEM ARM 200F TEM for transmission electron imaging. For *in vivo* studies, we excited the section of brain tissues at 405 nm and collected the fluorescence between 400 nm and 700 nm using an optical fiber that we positioned above different regions of the tissue.

2.3. Optical setup: spectral measurement of fluorescence. A pulsed diode laser emitting at 405 nm of 40 MHz with a power of 1 mw from PicoQuant (GmbH, Berlin, Germany) was used for excitation. A bi-fibered configuration was employed for excitation and collection positioned 1.5 mm above the specimen. The fibres used for excitation and collection had a core diameter of 200 µm and 365 µm, respectively, with a numerical aperture of 0.22. The spatial resolution was of 500 µm. Collected fluorescence signal was sent toward a computer controlled cooled spectrometer (Ocean optics QP600-1-UV-VIS) for spectroscopic analysis.[35] Spectral acquisition was accomplished for several longitudinal lines of each sample using a specific mechanical support mounted on a motorized micro-translator stage (Thorlabs, Newton, USA) and it lasted 5 to 10 minutes per sample.

2.4. Heating studies in solution. In a first experiment, the different suspensions were heated using a heating bath (QBD2, Grant) at different temperatures from 20 °C to 90 °C, for different times of 0 to 240 minutes. To verify that we have reached the desired temperature, we measured the temperatures of the suspensions using a thermocouple (physitemp, therms usb). Following heat treatment, we isolated the supernate from the nanoparticles using a Neodinum magnet that attracted the nanoparticles and we measured the absorption of the supernate. We then measured the absorption of the different suspensions between 400 nm and 700 nm containing 28 µg in iron of MC, MCR400, MC@RhB-1, and MC@RhB-2 in 1 mL (Figs. 2(a) to 2(c)). In a second experiment, the different suspensions were heated as described above and we measured: i), the absorption of suspensions containing 116 µg/mL of MC@RhB-1 or MCR400 or of their supernate for different heating times and heating temperatures (Figs. 3(a) to 3(c)), ii), the concentration of rhodamine B in the supernate after heat treatment of the MCR400 suspension

(Fig. 3(d)), iii), the fluorescence of the suspension containing 116 µg/mL in iron of MCR400 or 5 µM of rhodamine B, which was exited at 405 nm and fluorescence were collected between 550 and 650 nm, (Figs. 3(e), 3(f) and S1).

2.3. Irradiation studies in solution. Samples containing 400 µg/mL in iron oxide of MCR400 or 125 µM of rhodamine B were irradiated using a Faxitron irradiator dosimeter (160 kV, 6.3 mA and without filter, 67.5 Gy/min), using irradiation doses ranging from 0 to 1350 Gy. The fluorescence of the supernate of irradiated MCR400, obtained after magnetic separation, and of irradiated rhodamine B was measured (Fig. 4). Samples were exited at 405 nm and fluorescence was collected between 550 and 650 nm.

2.4. Fluorescence studies as a function of pH. pH of 1 mL suspensions containing MCR400, the supernate of MCR400, or rhodamine B was varied between 2 and 12 using a NaOH or HCl solution. The fluorescence spectra of these suspensions were then measured between 551 and 650 nm for 800 µl suspensions after excitation at 550 nm.

2.5 Cells. To isolate murine peritoneal macrophages, C57BL/6 were injected i.p. with zymosan (200 µl, 5mg/ml). Three days later, the mice were sacrificed and their peritoneal cavity washed with 4 ml of ice-cold PBS including 2 mM EDTA.

The murine fluorescent tumor cell line TC1-GFP[36] were maintained in culture in complete RPMI, including 10% FCS (GE Healthcare), antibiotics (Penicillin 50U/ml, Streptomycin 50 µg/ml, GIBCO), L-Glutamine (4 mM, GIBCO) and Sodium Pyruvate (1 mM, GIBCO).

RG2 cells were obtained from American Type Culture Collection. Cell lines were grown in Dulbecco's modified Eagle's medium (DMEM) supplemented with 10% fetal calf serum (FCS), 2 mM L-glutamine, 1 mM sodium pyruvate, 50 U/ml streptomycin (all obtained from Life Technologies Inc.), at 37 °C in a 5% CO2 humidified atmosphere, until they reached 90% confluency. The medium was removed and the cells were harvested using trypsin (0.04% trypsin / EDTA). The cells were centrifuged at 800 rpm for 5 min, suspended in PBS to final concentration of $3x10^3$ RG2 cells/µL.

U87-MG cells were obtained from American Type Culture Collection. Cell lines were grown in Dulbecco's modified Eagle's medium (DMEM) supplemented with 10% fetal calf serum (FCS), 2 mM L-glutamine, 1 mM sodium pyruvate, 50 U/ml streptomycin (all obtained from Life Technologies Inc.), at 37 °C in a 5% CO_2 humidified atmosphere, until they reached 90% confluency.

2.6 *In vitro* optical imaging studies. 2 10^4 TC1-GFP cells were seeded in a glass-bottomed culture dish (35 mm) for 24 hours, and treated with 350 µg/mL in iron oxide of MCR400 during 15 min. For fluorescence imaging, images were obtained with an inverted microscope (TE2000-E; Nikon) equipped with a 20x objective, and the Metamorph imaging software. Image analysis was done with Image J.

2.7 *In vitro* TEM studies. U87-Luc were seeded on a 12-well culture plate for 24h and treated with 3 µg/mL in iron. 10^6 from fixed cell suspensions were washed once with cacodylate buffer (0.1 M), fixed with glutaraldehyde (2.5%) at 4 °C for 60 min and washed with cacodylate buffer. Samples were then postfixed with 1% osmium tetroxide containing 1.5% potassium cyanoferrate, gradually dehydrated in ethanol (30%-100%) and embedded in Epon. Thin sections (80 nm) were collected onto 200 mesh cooper grids, and counterstained with lead citrate before examination with a Zeiss EM 902 transmission electron microscope at 80 KV (MIMA2-plateau de MET- unité 1196 GPL-Jouy-en-Josas). Microphotographies were acquired using Mega-View III CCD camera and analyzed with ITEM software (Eloïse SARL - Roissy CDG- France).

2.3. *In vivo* fluorescence studies. To evaluate if MCR400 can be used as pH probe *in vivo*, 4 rats were used. The rat 1 is a healthy rat euthanized at the same time as rat 2. Rats 2 to 4 received 5 µl of a suspension containing 3.10^3 RG-2 cells, implanted using a stereotactic helmet through the left hemisphere (2 mm lateral and anterior to bregma) to a depth of 4 mm. Rat 2 was not treated and euthanized 18 days after the implantation of the cells. Rats 3 and 4 received 14 µl of a suspension of MCR400 at a concentration of 668 µg/mL in iron oxide fourteen days following tumor cell implantation. Rats 3 and 4 were euthanized 2 hours and 4 days following MCR400 administration, respectively. Brains of these rats were then extracted and cut into 3 mm thick slices.

3. RESULTS AND DISCUSSION

Fluorescent magnetosomes were synthesized using three different methods that are summarized in the schematic diagrams of Scheme 1.

3.1 Preparation of dissociating probes: synthesis of fluorescent magnetosomes, designated as MCR400, by introducing rhodamine B in the growth medium of magnetotactic bacteria. Magnetotactic bacteria synthesize intracellular well-crystallized iron oxide nanoparticles with better magnetic properties than most chemically synthesized iron oxide nanoparticles.[37] This is achieved by introducing a source of iron in the growth medium of these bacteria, which penetrates inside these bacteria and crystallizes into nanominerals. In this work, the source of iron was mixed with a solution of 400 μM rhodamine B to produce fluorescent magnetosomes, designated as MCR400. Growth of magnetotactic bacteria was carried out as described in section 2.1, except that the source of iron was mixed with 400 μM of rhodamine B. Bacteria grow 7 days longer in the presence than in the absence of rhodamine B. Although whole magnetotactic bacteria as well as magnetosome chain arrangement and magnetosome shapes appear to be relatively similar for bacteria grown in the absence or presence of rhodamine B as shown in the TEM images of Figs. 1(a), 1(b), 1(d), 1(e), magnetosome sizes appear to be larger by 30-40% in the presence than in the absence of rhodamine B (Figs. 1(c) and 1(f)). This behavior may be attributed to the chelation of iron by rhodamine B that facilitates the introduction of iron inside magnetotactic bacteria.[38] Following growth, magnetosomes were extracted and separated from organic debris as described in section 2.1 for non-fluorescent magnetosomes and we obtained a suspension of fluorescent magnetosomes designated as MCR400 in which rhodamine B was associated to magnetosomes.

3.2 Preparation of non-dissociating probe: Synthesis of fluorescent magnetosomes, designated as MC@RhB-1, by chemically associating rhodamine B to chains of magnetosomes extracted from magnetotactic bacteria. 30 mg of rhodamine B was mixed with 3 mL of distilled water to produce a solution of rhodamine B at 0.0626 mmol. This solution was introduced in a three-necked round-bottom flask equipped with a thermometer, a condenser, a pH-meter, and a magnetic stirrer. Aqueous HCl solution (1 N) was added drop wise at 0°C to reach a pH of 4.5. Then, 24 mg of EDC ((3-

(Éthyliminométhylidèneamino)-N,N-diméthylpropan-1-amine) at 0.156 mmol and 18 mg of NHS ((1-hydroxypyrrolidine-2,5-dione) at 0.156 mmol were successively added to the rhodamine B solution kept at 0°C and pH = 4.5. The rhodamine B reaction mixture was then stirred for 4h at 0°C and pH = 4.5. 10 mL of a suspension of pH = 11.5 containing 3 mg of chains of magnetosomes extracted from magnetotactic bacteria (CM) mixed in distilled water were sonicated and added to the rhodamine B reaction mixture. pH was maintained at 11.5 using a 1N aqueous NaOH solution. The mixture was then stirred at 60°C during 22h. Then, the reaction was stopped by addition of an aqueous 1 N HCl solution until pH = 7 was reached. Magnetosomes associated to rhodamine B, designated as MC@RhB-1, were then concentrated using a strong Neodymium magnet (0.6 Tesla), re-suspended in 10 mL of sterile water and washed several times with sterile water using a magnet to isolate MC@RhB-1 from free rhodamine B. Finally, we used a chromatographic SEPHADEX G-25 gel (GE Healthcare, Buckimghamshire, UK) to isolate MC@RhB-1 from free residual compounds such as urea.

3.3 Preparation of non-dissociating probes: Synthesis of MC@RhB-2, by adsorbing rhodamine B at the surface of chains of magnetosomes extracted from magnetotactic bacteria. Suspensions of non-fluorescent chains of magnetosomes extracted from magnetotactic bacteria (MC) at 28 µg/mL in iron were mixed with a rhodamine B solution at four different concentrations of 120 ng/mL, 240 ng/mL, 3 µg/mL and 4µg/mL at pH 8. The mixed suspensions contained in 1 mL were sonicated using a finger at 5 W and 40°C during 2 hours. Magnetososomes were magnetically separated from the supernate 12 times using a Neodinim magnet as described above. Following each separation step, the supernate containing free rhodamine in excess was removed and nanoparticles were re-suspended in water. For the lowest quantity of rhodamine B of 120 ng, we did not observe any significant peak from rhodamine B in the absorption spectra of the mixed suspensions after 1 or 12 separation steps (Fig. S2(a)). When the quantity of rhodamine B was increased, the spectra of MC mixed with rhodamine B followed by one separation step show a peak at rhodamine B absorption wavelength for quantities of rhodamine B of 240 ng (Fig. S2(b)), 2.6 µg (Figs. S2(c)), 3.9 µg (Fig. S2(d)). However, this peak disappears after 12

separation steps (Figs. S2(b) to S2(d)), indicating that rhodamine B is not adsorbed to the magnetosomes in MC@RhB-2.

3.4 Type of fluorescent magnetosomes that can be used as dissociating probe.

To prepare the suspensions containing the three-different fluorescent magnetosomes, MCR400, MC@RhB-1, and MC@RhB-2, we isolated the nanoparticles from the supernate of the nanoparticle suspensions by positioning a Neodymium magnet against the Eppendorf tube containing 1 mL of these suspensions, we removed the supernate that we replaced by 1 mL of water. This corresponded to the first separation step and this step was repeated 12 times. During each separation step, we measured the optical density of the supernate at 550 nm to examine the presence or not of rhodamine B in the supernate. Fig. 2(a) shows that the optical density of the supernate either progressively decreases between the first and fifth separation step to becomes negligible afterwards for MCR400 and MC@RhB-1 or disappears immediately after the first separation step for MC@RhB-2. This indicates that after 12 separation steps, the supernates of the three nanoparticle suspensions do not contain any rhodamine B. Given that we define the association between rhodamine B and the magnetosomes as that, which can withstand magnetic separation, we deduce that after 12 separation steps if rhodamine B molecules remain in MCR400, MC@RhB-1, and MC@RhB-2 suspensions, they are associated with the magnetosomes. After 12 separation steps, the signal of fluorescence of the supernate was negligible at the emission wavelengths of rhodamine B, confirming the absence of free rhodamine B in the supernate.

We further examine if the suspensions containing MCR400, MC@RhB-1, and MC@RhB-2, which were obtained after 12 separation steps, can be used as a dissociating probe. In both absorption and fluorescent spectra of MC@RhB-2, rhodamine B peaks are absent (Figs. 2(b) and 2(c)), indicating that rhodamine B has not associated to the magnetosomes in this sample (Fig. S2) and that MC@RhB-2 can therefore not be used as fluorescent probe. By contrast, for MC@RhB-1, although the absorption spectrum is similar to that of MC (Fig. 2(b)), suggesting that large numbers of rhodamine B molecules are not associated to the magnetosomes, the fluorescence spectrum of MC@RhB-1 is similar to that of rhodamine B (Fig. 2(c)), indicating that rhodamine B is associated to the magnetosomes in MC@RhB-1.

However, when we heated the MC@RhB-1 suspension during 30 minutes at 90 °C, collected its supernate by magnetic separation and measured the absorption spectrum of the supernate (Fig. 3(a)), we observed that the absorption peak of rhodamine B was absent (Fig. 3(a)), suggesting that rhodamine B has not dissociated from the magnetosomes following heating and that MC@RhB-1 could therefore not be used as a dissociating probe. For MCR400, the association of rhodamine B to the magnetosomes was highlighted on the one hand by the absorption spectrum of the MCR400 suspension, which displays a shoulder at 550 nm corresponding to the maximum absorption wavelength of rhodamine B (Fig. 2(b)) and by the fluorescence emission spectrum of the same suspension, which shows a peak with maximum fluorescence intensity at 569 nm (Fig. 2(c)), a wavelength that is slightly lower than that corresponding to the maximum fluorescence intensity of rhodamine B at 581 nm (Fig. 2(c)). Indeed, the difference in emission wavelength between free rhodamine and MCR400 could be explained by the association of rhodamine B to the nanoparticles, since this type of shift has previously been observed with fluorophores entrapped into nanoparticles.[38] Furthermore, when the MCR400 suspension was heated during 30 minutes at 90 °C and its supernate was magnetically separated from the nanoparticles, we measured that the absorption of the supernate displays a peak at 555 nm (Fig. 3(b)), a similar wavelength as that of free rhodamine B (Fig. 2(b)), indicating that rhodamine B has dissociated from the magnetosomes after heating and that MCR400 could therefore be used as a dissociating probe.

3.5 Quantity of rhodamine B associated to magnetosomes in MCR400.

To further characterize MCR400, we determined the number of rhodamine B molecules associated to each magnetosome in MCR400. For that, the pH of the MCR400 suspension was decreased to 2 using hydrochloric acid, leading to the release of rhodamine B from the magnetosomes. The fluorescence and absorption properties of MCR400 and free rhodamine B brought to pH 2 are presented in Fig. S3. The spectrum of MCR400 at pH 2 (Fig. S2(c)) shows a peak at 582 nm, which corresponds to the emission wavelength of free rhodamine B in solution at pH 2, confirming that rhodamine B has been released from the magnetosomes after a change in pH. From the intensity of this peak of ~ 0.56 a.u (Fig. S2(c)), we have deduced a rhodamine B concentration of 750 nmol/L using a calibration curve, which

represents the variation of rhodamine B fluorescence intensity at pH = 2 as a function rhodamine B concentration (Fig. S2(a)). Given a magnetosome concentration of 166 µg/mL, a magnetosome weight of 6.25×10^{-16} g, a number of rhodamine B molecules and magnetosomes per mL of 4.6×10^{14} and 26.5×10^{10}, respectively, we have deduced that 178 ± 4 rhodamine B molecules were associated to each magnetosome on average. Rhodamine B molecules are more likely adsorbed at magnetosome surface to enable their release within the magnetosome surrounding environment, but vacancies may also be present in the magnetosome mineral crystal core, which could possibly be filled with rhodamine B molecules.

3.6 Dissociation of rhodamine B from the magnetosomes with increasing temperatures in suspensions of MCR400.

To examine if rhodamine B dissociation from the magnetosomes is enhanced with increasing temperature, we first measured the optical density at 550 nm of the supernates of MCR400 suspensions, which were heated at 20 °C to 90 °C for 0 to 240 minutes. For the three heating temperatures of 20 °C, 60 °C, and 90 °C, the optical density at the absorption wavelength of rhodamine B (550 nm) of the supernate of MCR400 has been measured as a function of heating time. For these three temperatures, Fig. 3(c) shows that the optical density saturates after 100 minutes of heating at 0.004 (20 °C), at 0.028 (60 °C), at 0.048 (90 °C). To make sure that saturation was reached, MCR400 suspensions were then heated during 240 minutes at various temperatures and we observed that rhodamine B concentration in the supernate of MCR400 increased from 20 nM at 20 °C to 560 nM at 90 ºC, where these concentrations were determined using the calibration curve of free rhodamine B (Fig. S3(b)). Given that 41.5 molecules of rhodamine B per magnetosomes are in the supernate at 90 °C, and that there are 178 rhodamine B molecules per magnetosome before heating, we deduce that 23% of rhodamine B have dissociated from the magnetosomes at 90 °C.

We then studied if MCR400 could be used as a fluorescent temperature probe. For that, we measured the fluorescence spectra of a MCR400 suspension heated at 20 °C, 35 °C, 50 °C, 65 °C, and 80 °C (Fig. 3(e)) and we observed that the maximum fluorescence intensity of the emission peak, at 569 nm,

strongly increases by 66% (Fig. 3(e)) with increasing temperature, a behavior which is the opposite to that of free rhodamine B whose fluorescence intensity is observed to sharply decrease by 73% with increasing temperature within this temperature range, (Fig 3(f)).[39] In MCR400, the fluorescence intensity of rhodamine B would initially be attenuated when rhodamine B is associated to the magnetosomes, most probably due to quenching by iron oxide[40], and would then increase when rhodamine B dissociates from the magnetosomes with increasing temperature. Using the relation between MCR400 fluorescence intensity and temperature, it therefore appears feasible to use MCR400 fluorescence as a temperature probe.

3.6 Dissociation of rhodamine B from the magnetosomes by exposing MCR400 to radiation.

To examine if rhodamine B dissociates from the magnetosomes under radiation, we have irradiated a suspension of MCR400 at doses ranging from 0 Gy to 1350 Gy. The supernate of this suspension was isolated from the nanoparticles by magnetic separation and we measured its fluorescence intensity at 578 nm, corresponding to the emission wavelength of free rhodamine B. The fluorescence intensity was observed to strongly increase by a factor of ~ 2-4 from 200-300 a.u. in the absence of irradiation to 600-900 a.u. at 300-1350 Gy (Fig. 4). Given that the luminescence intensity of free rhodamine B does not vary with increasing radiations (Fig. 4), the behavior of MCR400 observed in Fig. 4 could be attributed to the dissociation of rhodamine B from the magnetosomes under radiations.

3.8 Dissociation of rhodamine B from the magnetosomes at acidic pH in MCR400 suspensions

Next, to examine if MCR400 can be used as a pH probe, we have adjusted the pH of a MCR400 suspension containing 400 μg/mL of iron oxide to values between 2 and 12 by adding a 0.1 to 12 M hydrochloric acid or sodium hydroxide solution. The samples containing the treated MCR400 were then placed against a magnet of 0.6 T for 12 h at 4 °C and the supernate was collected. At acidic pH, the maximum fluorescence intensity of MCR400 and of its supernate increases with decreasing pH (Fig. 5(a)), a behavior opposite to that observed for free rhodamine B suggesting that MCR400 release free rhodamine B in the supernate at acidic pH. Between pH 8 and 12, the fluorescence intensity of the MCR400 suspension and of its supernate increase much less than at acidic pH (Fig. 5(a)). These

behaviors suggest that rhodamine B dissociates from MCR400 much more significantly at acidic than basic pH. This conclusion is further supported by the analysis of the wavelength variation with pH. Indeed, at basic pH (pH > 7), we observe that the emission wavelength of MCR400 is lower than that of free rhodamine B or of MCR400 supernate, suggesting that most rhodamine B molecules have not been dissociated from the magnetosomes to yield free rhodamine B. In this case, MCR400 may have formed a complex containing magnetosomes and rhodamine B. By contrast, at acidic pH (pH < 7), Fig. 5(b) shows that the emission wavelengths of MCR 400 increases with decreasing pH to reach the same value as that of free rhodamine at pH 2. To conclude, MCR400 may be used to locally measure pH in acidic but not basic conditions.

3.9 MCR400 as *in vitro* probe.

Zymosan-elicited, peritoneal macrophages can rapidly internalize MCR400, presumably by phagocytosis. Fig 6 (a) shows that red fluorescent MCR400 particles accumulate in intracellular vesicles macrophage. Another type of cell was used to determine if this behavior could be generalized to different cell types. As shown in Fig. 6(b), when MCR400 are incubated with TC1-GFP tumor cells for 15 minutes, fluorescence imaging reveals the same localized red spots as in Fig. 6(a). It clearly appears that these intracellular vesicles are cytoplasmic, and not nuclear. Further evidence of the localization of the magnetosomes inside intracellular vesicles was provided by an electron microscopy image of a TC1-GFP incubated with MCR400 (Fig. 6(c)), which clearly shows that magnetosomes are concentrated in intracellular vesicles (an assembly of 18 magnetosomes in this case) and not dispersed in the cytoplasm.

3.10 MCR400 as *in vivo* probe

For the different rats, fluorescent spectra of the healthy areas without MCR400, presented in Figures 7(a) to 7(d), are very similar with a broad peak of maximum intensity at ~500 nm, which is attributed to the combination of nicotinamide dinucleotide (NADH) and flavins (FAD), occurring at 450 nm and 525 nm, respectively.[38,41] This peak display three shoulder at 575 nm, 625 nm, and 690 nm, possibly due to the fluorescence of the lipopigments, the porphyrins and the chlorins respectively.[43] The spectra of the healthy areas were averaged, thus making it possible to normalize all the fluorescence spectra measured

for all the slices of rat brain. The auto-fluorescent spectra of tumor areas appear to be similar than those of healthy areas, except that peak intensities are weaker. For rat 3 euthanized two hours following MCR400 administration, the fluorescence spectrum of the tumor region, in which MCR400 were administrated, show the presence of two interesting peaks, at 569 nm and 576 nm which are either absent or less intense relatively to the emission at 500 nm in the spectra of the tumor and healthy regions. We attribute these two peaks to the emission of MCR400 at 569 nm which was similar in solution and to that of rhodamine B and lipo-pigment at 576 nm, both emitting at this wavelength. In the region containing MCR400, the peak at 576 nm can not only be due to the endogenous fluorescence of the lipopigments, since its fluorescence intensity at 576 nm relatively to that at 500 nm, $I_{576}/I_{500} \sim 1$, is higher than that of $I_{576}/I_{500} \sim 0.5$ measured for healthy and tumor areas without MCR400. For rat 4 euthanized four days following MCR400 administration, the fluorescence spectrum of the tumor region with MCR400 also shows a peak at 576 nm with enhanced intensity, suggesting the presence of free rhodamine B released from the magnetosomes. The peak at 569 nm attributed to MCR400 has disappeared, which could be due the dissociation of all rhodamine B from the magnetosomes 4 days after MCR400 administration.

3. CONCLUSION:

In conclusion, we have shown that intruding 400 μM of rhodamine B in the growth medium of AMB-1 magnetotactic bacteria leads to the production of magnetosomes of larger sizes than in the absence of rhodamine B, possibly due to the chelation of iron by rhodamine B. After extraction form magnetotactic bacteria, these magnetosomes appear to be fluorescent with absorption and emission peaks at similar wavelengths than those of free rhodamine B. When they are heated to 30-90 °C, brought to acidic pH, or exposed to radiations (> 300 Gy), these magnetosomes also appear to release rhodamine B. Furthermore, when they are mixed *in vitro* with tumor cells (TC1-GFP or RG2 cells) or introduced in the brains of rats, fluorescence intensity is enhanced at rhodamine B emission wavelength, possibly due to magnetosomes being captured by cells which may in turn lead to rhodamine B release. We have developed a fluorescent probe that works by dissociation of the fluorescent molecules (rhodamine B)

from the nanoparticles (magnetosomes). Compared with other fluorescent probes without any dissociating mechanism, our probe presents the advantage of potentially enabling the simultaneous monitoring and control of drug release from nanoparticles. Such probe was not described before.[43] Since typical commonly used cancer drugs such as doxorubicin have a similar molecular weight than rhodamine B and possess chelating chemical functions, it is possible to imagine that they could replace rhodamine B and improve the magnetic hyperthermia treatment of tumors, by combing the effect of heat with that of drug activation.[44,45,46]

Acknowledgment: We would like to thank the Eurostars program (Nanoneck-2, E9309), subvention AIR from the region of Paris (A1401025Q), the ANR Méfisto as well as the ANRT (CIFRE 2014/0359). Edouard Alphandéry wrote the article and directed the research described in this article.

REFERENCES:

1. Chekina, N.; Horák, D.; Jendelová, P.; Trchová, M.; Beneš, M.-J.; Hrubý, M.; Herynek, V.; Turnovcova, K.; Sykova, E. Fluorescent magnetic nanoparticles for biomedical applications. *J. Mater Chem.* **2011**, 21, 7630–9.

2. Benjaminsen, R.-V.; Sun, H.; Henriksen, J.-R.; Christensen, N.-M.; Almdal, K.; Andresen, T.-L.; Evaluating Nanoparticle Sensor Design for Intracellular pH Measurements. *ACS Nano*. **2011**, 26,5864–5873.

3. Bai, Z.; Chen, R.; Si, P.; Huang, Y.; Sun, H.; Kim, D.-H. Fluorescent pH Sensor Based on Ag@SiO2 Core–Shell Nanoparticle. *ACS Appl Mater Interfaces*. **2013**, 5, 5856–60.

4. Susha, A.-S.; Javier, A.-M.; Parak, W.-J.; Rogach A.-L. Luminescent CdTe nanocrystals as ion probes and pH sensors in aqueous solutions. Colloids and Surfaces A: Physicochemical and Engineering Aspects.*Colloids AND Surfaces A.* **2006**, 281, 40–43.

5. Bertorelle, F.; Wilhelm, C.; Roger, J.; Gazeau, F.; Ménager, C.; Cabuil, V. Fluorescence-Modified Superparamagnetic Nanoparticles: Intracellular Uptake and Use in Cellular Imaging. *Langmuir*. **2006**, 22, 5385–5391.

6. Li, X.; Chen L. Fluorescence Probe Based on an Amino-Functionalized Fluorescent Magnetic Nanocomposite for Detection of Folic Acid in Serum. *ACS Appl. Mater Interfaces.* **2016**, 8, 31832–31840.

7. Basuki, J.-S.; Duong, H.-T.-T.; Macmillan, A.; Erlich, R.-B.; Esser, L.; Akerfeldt, M.-C..; Megan W.-R.; Kavallaris, M.; Boyer, C.; Davis T.-P.. Using Fluorescence Lifetime Imaging Microscopy to Monitor Theranostic Nanoparticle Uptake and Intracellular Doxorubicin Release. *ACS Nano*. **2013**, 7, 10175–101789.

8. Chen, J.; Zheng, A.; Chen, A.; Gao, Y.; He, C.; Kai, X.; Wu, G.; Chen, Y. A functionalized gold nanoparticles and Rhodamine 6G based fluorescent sensor for high sensitive and selective detection of mercury(II) in environmental water samples. *Analytica Chimica Acta.* **2007**, 599, 134–142.

9. Arai, S.; Lee, S.-C.; Zhai, D.; Suzuki, M.; Chang, Y.-T. A Molecular Fluorescent Probe for Targeted Visualization of Temperature at the Endoplasmic Reticulum. *Scientific Reports.* **2014**, 4, 6701.

10. Freddi, S.; Sironi, L.; D'Antuono, R.; Morone, D.; Donà, A.; Cabrini, E.; D'Alfonso, L.; Collini, M.; Pallavicini, P.; Baldi, G.; Maggioni, D.; Chirico, G.; A Molecular Thermometer for Nanoparticles for Optical Hyperthermia. *Nano Lett.* **2013**, 13, 2004–2010.

11. Cui, J.; Kwon, JE.; Kim, H-J.; Whang, DR.; Park, SY. Smart Fluorescent Nanoparticles in Water Showing Temperature-Dependent Ratiometric Fluorescence Color Change. *ACS Appl Mater Interfaces.* **2017**, 9, 2883–2890.

12. Ali, H.; Bhunia, S.-K.; Dalal, C.; Jana, N.-R. Red Fluorescent Carbon Nanoparticle-Based Cell Imaging Probe. *ACS Appl Mater Interfaces.* **2016**, 8, 9305–9313.

13. Das, P.; Jana, N.-R.; Highly Colloidally Stable Hyperbranched Polyglycerol Grafted Red Fluorescent Silicon Nanoparticle as Bioimaging Probe. *ACS Appl Mater Interfaces.* **2014**, 6, 4301–4309.

14. Fan, Z.; Sun, L.; Huang, Y.; Wang, Y.; Zhang, M. Bioinspired fluorescent dipeptide nanoparticles for targeted cancer cell imaging and real-time monitoring of drug release. *Nat. Nano.* **2016**, 11, 388–394.

15. Wolfbeis O.-S. An overview of nanoparticles commonly used in fluorescent bioimaging. *Chemical Society Reviews.* **2015**, 44, 4743–4368.

16. Colby, A.-H.; Berry, S.-M.; Moran, A.-M.; Pasion, K.-A.; Liu, R.; Colson, Y.-L.; Ruiz-Opazo, N.; Grinstaff, M.-W.; Herrera, V.-L. Highly Specific and Sensitive Fluorescent Nanoprobes for Image-Guided Resection of Sub-Millimeter Peritoneal Tumors. *ACS Nano.* **2017**, 11, 1466–1477.

17. Al-Kady, A.-S.; Gaber, M.; Hussein, M.-M.; Ebeid, E.-Z.-M. Structural and fluorescence quenching characterization of hematite nanoparticles. *Spectrochimica Acta Part A: Molecular and Biomolecular Spectroscopy.* **2011**, 83, 398–405.

18. Yu, C-J.; Wu, S.-M.; Tseng, W.-L. Magnetite Nanoparticle-Induced Fluorescence Quenching of Adenosine Triphosphate–BODIPY Conjugates: Application to Adenosine Triphosphate and Pyrophosphate Sensing. *Anal Chem.* **2013**, 85, 8559–65.

19. Simard, B.; Tomanek, B.; Van Veggel, F.-C.-J.-M.; Abulrob, A. Optimal dye-quencher pairs for the design of an "activatable" nanoprobe for optical imaging. Photochem. *Photobiol Sci.* **2013**, 12, 1824–1829.

20. Lei, G.; Gao, P.-F.; Yang, T.; Zhou, J.; Zhang, H.-Z.; Sun, S.-S.; Gao, M.-X.; Zhi Huang C. Photoinduced Electron Transfer Process Visualized on Single Silver Nanoparticles. *ACS Nano.* **2017**, 11, 2085–2093.

21. Alphandéry, E.; Walsh, L.-M.; Rakovich, Y.; Bradley, A.-L.; Donegan, J.-F.; Gaponik, N. Highly efficient Förster resonance energy transfer between CdTe nanocrystals and Rhodamine B in mixed solid films. *Chemical Physics Letters.* **2004**, 388, 100–104.

22. Sapsford, K.-E.; Berti, L.; Medintz, I.-L. Materials for Fluorescence Resonance Energy Transfer Analysis: Beyond Traditional Donor–Acceptor Combinations. *Angewandte Chemie International Edition.* **2006**, 45, 4562–4589.

23. Pal, M.; Rakshit, R.; Mandal, K. Surface Modification of MnFe2O4 Nanoparticles to Impart Intrinsic Multiple Fluorescence and Novel Photocatalytic Properties. *ACS Appl Mater Interfaces.* **2014**, 6, 4903–4910.

24. Hong, H.; Wang, F.; Zhang, Y.; Graves, S.-A.; Eddine, S.-B.-Z.; Yang, Y.; Theuer, C.-P.; Nickles, R.-J.; Wang, X.; Cai, W. Red Fluorescent Zinc Oxide Nanoparticle: A Novel Platform for Cancer Targeting. *ACS Appl Mater Interfaces.* **2015**, 7, 3373–3381.

25. Tan, X.; Wang, J.; Pang, X.; Liu, L.; Sun, Q.; You, Q.; Tan, F.; Li, N. Indocyanine Green-Loaded Silver Nanoparticle@Polyaniline Core/Shell Theranostic Nanocomposites for Photoacoustic/Near-Infrared Fluorescence Imaging-Guided and Single-Light-Triggered Photothermal and Photodynamic Therapy. *ACS Appl Mater Interfaces.* **2016**, 8, 34991–35003.

26. Bazylinski, D.-A.; Frankel, R.-B. Magnetosome formation in prokaryotes. *Nat Rev Micro.* **2004**, 2, 217–230.

27. Alphandéry, E.; Faure, S.; Seksek, O.; Guyot, F.; Chebbi, I. Chains of Magnetosomes Extracted from AMB-1 Magnetotactic Bacteria for Application in Alternative Magnetic Field Cancer Therapy. *ACS Nano.* **2011**, 5, 6279–6296.

28. Alphandéry, E.; Chebbi, I.; Guyot, F.; Durand-Dubief M. Use of bacterial magnetosomes in the magnetic hyperthermia treatment of tumours: A review. *International Journal of Hyperthermia.* **2013**, 29, 801–809.

29. Alphandéry, E. Applications of Magnetosomes Synthesized by Magnetotactic Bacteria in Medicine. *Front. Bioeng. Biotechnol*. [Internet]. **2014** Mar 11 [cited 2017 May 26];2. Available from: http://www.ncbi.nlm.nih.gov/pmc/articles/PMC4126476/

30. Alphandéry, E.; Lijeour, L.; Lalatonne, Y.; Motte, L. Different signatures between chemically and biologically synthesized nanoparticles in a magnetic sensor: A new technology for multiparametric detection. *Sensors and Actuators B: Chemical.* **2010**, 147, 786–790.

31. Lang, C.; Schüler, D. Expression of Green Fluorescent Protein Fused to Magnetosome Proteins in Microaerophilic Magnetotactic Bacteria. *Appl. Environ. Microbiol.* **2008**, 74, 4944–4953.

32. Carillo, M.-A.; Bennet, M.; Faivre D. Interaction of Proteins Associated with the Magnetosome Assembly in Magnetotactic Bacteria As Revealed by Two-Hybrid Two-Photon Excitation Fluorescence Lifetime Imaging Microscopy Förster Resonance Energy Transfer. *J. Phys. Chem. B.* **2013**, 117, 14642–14648.

33. Tang, T.; Zhang, L.; Gao, R.; Dai, Y.; Meng, F.; Li, Y. Fluorescence imaging and targeted distribution of bacterial magnetic particles in nude mice. *Appl. Microbiol. Biotechnol.* **2012**, 94, 495–503.

34. Alphandéry, E.; Amor, M.; Guyot, F.; Chebbi, I. The effect of iron-chelating agents on *Magnetospirillum magneticum* strain AMB-1: Stimulated growth and magnetosome production and improved magnetosome heating properties. *Appl. Microbiol. Biotechnol.* **2012**, 96, 663-670.

35. Leh, B.; Siebert, R.; Hamzeh, H.; Menard, L.; Duval, M-A.; Charon, Y.; Abi-Haidar, D. Optical phantoms with variable properties and geometries for diffuse and fluorescence optical spectroscopy. *J Biomed Opt.* **2012**, 17, 108001.

36. Thoreau M.; Penny, H.-L.; Tan, K.; Regnier, F.; Weiss, J.-M.; Lee, B.; Johannes, L.; Dransart, E.; Le Bon, A.; Abastado, J.-P.; Tartour, E.; Trautmann, A.; Bercovici, N. Vaccine-induced tumor regression requires a dynamic cooperation between T cells and myeloid cells at the tumor site. *Oncotarget.* **2015**, 6, 27832–27846.

37. Alphandéry, E. Perspectives of Breast Cancer Thermotherapies. *J. Cancer.* **2014**, 5, 472–479.

38. Auger, A.; Samuel, J.; Poncelet, O.; Raccurt, O. A comparative study of non-covalent encapsulation methods for organic dyes into silica nanoparticles. *Nanoscale Research Letters*. **2011**, 6, 328.

39. Kubin, R.-F.; Fletcher, A.-N. Fluorescence quantum yields of some rhodamine dyes. *Journal of Luminescence.* **1982**, 27, 455–62.

40. Turro, N.-J.; Lakshminarasimhan, P.-H.; Jockusch, S.; O'Brien, S.-P.; Grancharov, S.-G.; Redl, F.-X. Spectroscopic Probe of the Surface of Iron Oxide Nanocrystals. *Nano Lett.* **2002**, 2, 325–328.

41. Huang, S.; Heikal, A.-A.; Webb, W.-W. Two-photon fluorescence spectroscopy and microscopy of NAD(P)H and flavoprotein. *Biophys J.* **2002**, 82, 2811–2825.

42. Haidar, D.-A.; Leh, B.; Zanello, M.; Siebert, R. Spectral and lifetime domain measurements of rat brain tumors. *Biomed Opt Express.* **2015**, 6, 1219–1233.

43. Hergta, R.; Hiergeista, R.; Zeisbergera, M.; Schuler, D.; Heyen, U.; Hilger, I.; Kaiser, W.-A. Magnetic properties of bacterial magnetosomes as potential diagnostic and therapeutic tools. *J. Magn. Magn. Mat.* **2005**, 293, 80-86.

44. Le Fèvre1, R.; Durand-Dubief, M.; Chebbi, I.; Mandawla, C.; Lagroix, F.; Valet, J-P.; Idbaih, A.; Adam, C.; Delttre, J-Y.; Scmitt, C.; Maake, C.; Guyot, F.; Alphandéry, E. Enhanced antitumor efficacy of biocompatible magnetosomes for the magnetic hyperthermia treatment of glioblastoma. *Theranostics.* **2017**, doi:10.7150/thno.18927.

45. Alphandéry, E.; Idbaih, A.; Adam, C.; Delattre, J-Y.; Schmitt, C.; Guyot, F.; Chebbi, I. Chains of magnetosomes with controlled endotoxin release and partial tumor occupation induce full destruction of intracranial U87-Luc glioma in mice under the application of an alternating magnetic field. *J. Controlled. Release*. **2007**, 262, 259-272.

46. Alphandéry, E.; Idbaih, A.; Adam, C.; Delattre, J-Y.; Schmitt, C.; Guyot, F.; Chebbi, I. Development of non-pyrogenic magnetosome minerals coated with poly-L-lysine leading to full disapperance of intracranial U87-Luc glioblastoma in 100% of treated mice using magnetic hyperthermia. *Biomaterials.* **2017**, 141, 210-222.

CAPTIONS AND FIGURES:

Scheme 1: Schematic diagrams showing the steps involved in the preparations of: (a), the dissociating probe (MCR400) obtained by cultivating magnetotactic bacteria in the presence of 400 μM of rhodamine B and by extracting fluorescent chains of magnetosomes from these bacteria, (b), the non-dissociating probe (MC@RhB-1) obtained by extracting chains of magnetosomes from magnetotactic bacteria and by chemically attaching rhodamine B to the chains of magnetosomes, (c), the non-dissociating probe (MC@RhB-2) obtained by extracting chains of magnetosomes from magnetotactic bacteria and by adsorbing rhodamine B to the chains of magnetosomes.

Figure 1: For magnetotactic bacteria cultivated in the presence of 400 μM of rhodamine B, electron microscopic images of a whole magnetotactic bacterium, (a), a chain of magnetosomes contained inside

such bacterium, (b), and a histogram representing magnetosome size distribution inside such bacterium, (c). For magnetotactic bacteria cultivated in the absence of rhodamine B, electron microscopic images of a whole magnetotactic bacterium, (d), a chain of magnetosomes contained inside such bacterium, (e), and a histogram representing magnetosome size distribution inside such bacterium, (f). In (c) and (f), the histogram were realized on 300 magnetosomes (20 bacteria).

Figure 2: (a), variation of the optical density, measured at 550 nm, of the supernate of 1 mL suspensions containing 400 µg of MC@RhB-1, MC@RhB-2, MCR400, as a function of the number of separation step. (b), Absorption spectra of 1 mL suspensions containing 40 µg of MC, MCR400, MC@RhB-1, MC@RhB-2, or 4 µg of rhodamine B. The intensity of the MC@RhB-1 is divided by a factor of 1.6. (c), Fluorescence spectra, excited at 405 nm, of 800 µL suspensions containing 166 µg of MC, MCR400, MC@RhB-1, MC@RhB-2, or 0.4 µg of rhodamine B.

Figure 3: Absorption spectra of 1 mL suspensions containing 40 µg of MC@RhB-1, the supernate of this suspension obtained after magnetic separation, (a), a 1 mL suspension containing 40 µg of MCR400, the supernate of this suspension obtained after magnetic separation, (b), where the MCR400 and MC@RhB-1 suspensions have been heated at 90 °C during 15 minutes. (c), Optical density, measured at 550 nm, of the supernate of a 1 mL suspension containing 40 µg of MCR400 collected after the MCR400 suspension has been heated at 20 °C, 60 °C, 90 °C for different times varied between 0 and 240 minutes. (d), Concentration of rhodamine B in the supernate of a 1 mL suspension containing 40 µg of MCR400 collected after the MCR400 suspension has been heated at 20 to 90 °C during 240 minutes. (e), Fluorescence spectra, excited at 405 nm, of 1 mL suspensions containing 166 µg of MCR400, which have been heated at various temperatures of 20 °C, 35 °C, 50 °C, 65 °C, 80 °C, during 15 minutes. (f), Fluorescence spectra, excited at 405 nm, of 1 mL suspensions containing 40 µg of rhodamine B, which have been heated at various temperatures of 20 °C, 40 °C, 60 °C, 80 °C, during 15 minutes.

Figure 4: Fluorescence intensity, excited at 405 nm, measured at 576 nm, of the supernate of 1 mL suspensions containing 400 µg of MCR400 or 40 µg of free rhodamine B following irradiation at different doses varied between 0 Gy and 1350 Gy.

Figure 5: (a), Maximum fluorescence intensity of fluorescence spectra of 1 mL suspensions containing 400 µg of MCR400, the supernate of this suspension, or 40 µg of rhodamine B, excited at 405 nm and measured between 550 nm and 650 nm as a function of the pH of these suspensions varied between 2 and 12. (b), For the same suspensions, wavelength corresponding to the maximum fluorescence intensity as a function of the pH of these suspensions varied between 2 and 12.

Figure 6: MCR400 magnetosomes can efficiently be endocytosed or phagocytosed by macrophages and in tumor cells. (a), Zymozan-activated murine peritoneal macrophages were incubated with rhodamine-coupled MCR400 and imaged with a fluorescent optical microscope with excitation at 560 nm and 607 nm detection. During the first hour, a red fluorescence increased in the cells, under the form of red spots (yellow arrows) presumably corresponding to phagosomes. (b), TC1-GFP tumor cells incubated with MCR400 were imaged in the same conditions, plus the appropriate GFP filters (485 and 525 nm). Within less than an hour, the red fluorescence increased in the cytoplasm of TC1-GFP cells. (c), TEM image of a U87-Luc cell incubated with MCR400 for 15 minutes, where the cell was included in a resin and cut in an 80 nm thick slide with a microtome. The zoom represents a cell compartment, possibly a lysosome, phagosome, or endosome, containing MCR400.

Figure 7: Fluorescence spectra of different section of rat brain with an excitation at 405 nm and an emission between 400 et 725 nm. Spectra of two regions of a healthy brain without MCR400 administration, (a), Spectra of tumor region and healthy region without MCR400 administration, (b), Spectra of tumor region containing or not MCR400 and an Healthy region without MCR400, for a rat euthanized two hours following MCR400 administration (c), Spectra of tumor region containing or not MCR400 and an Healthy region without MCR400, for a rat euthanized 4 days following MCR400 administration, (d).

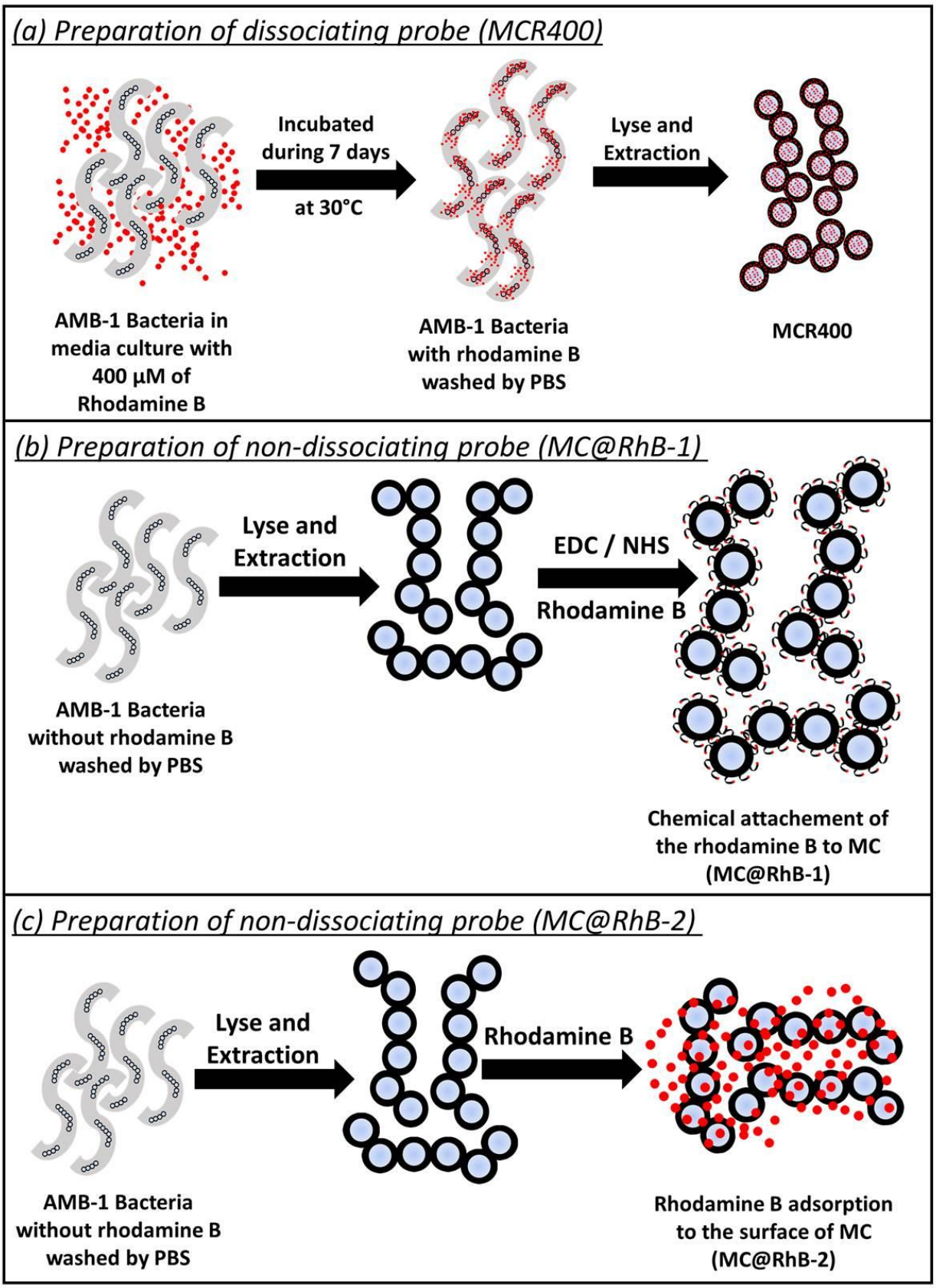
(a) Preparation of dissociating probe (MCR400)
Incubated during 7 days at 30°C
Lyse and Extraction
AMB-1 Bacteria in media culture with 400 µM of Rhodamine B
AMB-1 Bacteria with rhodamine B washed by PBS
MCR400
(b) Preparation of non-dissociating probe (MC@RhB-1)
Lyse and Extraction
EDC / NHS
Rhodamine B
AMB-1 Bacteria without rhodamine B washed by PBS
Chemical attachement of the rhodamine B to MC (MC@RhB-1)
(c) Preparation of non-dissociating probe (MC@RhB-2)
Lyse and Extraction
Rhodamine B
AMB-1 Bacteria without rhodamine B washed by PBS
Rhodamine B adsorption to the surface of MC (MC@RhB-2)

Scheme 1

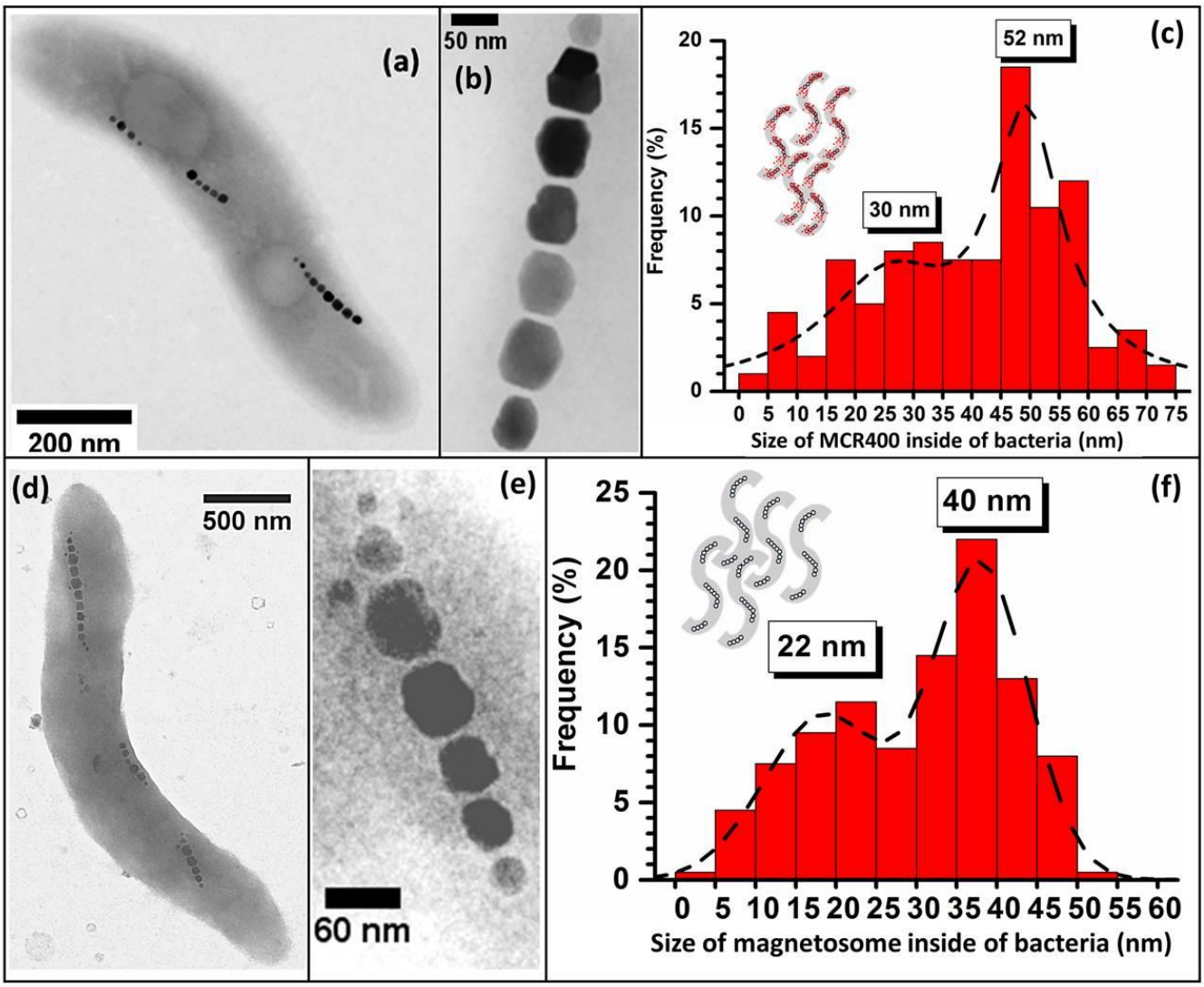
(a)
200 nm
50 nm
(b)
(c)
52 nm
30 nm
Frequency (%)
Size of MCR400 inside of bacteria (nm)
(d)
500 nm
(e)
60 nm
(f)
40 nm
22 nm
Frequency (%)
Size of magnetosome inside of bacteria (nm)

Figure 1

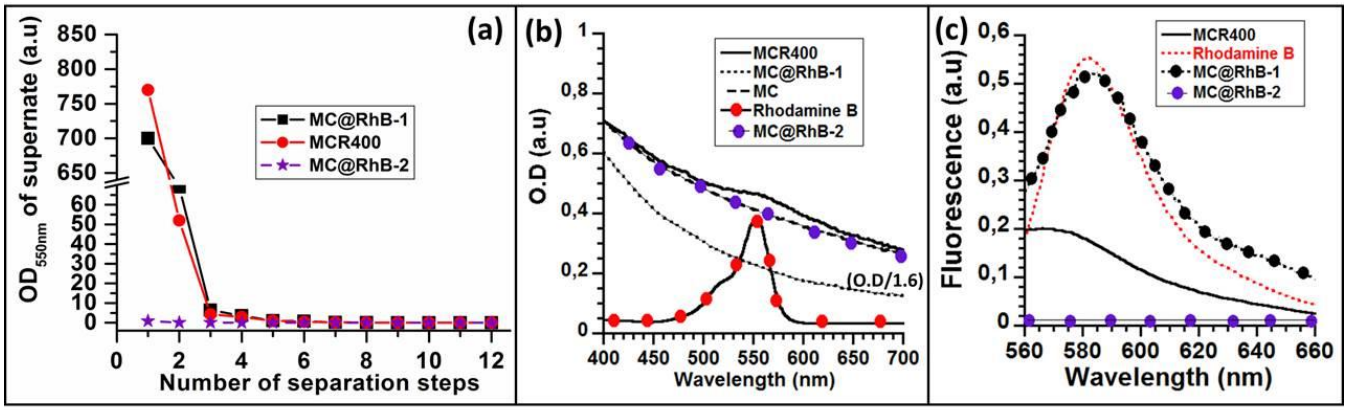
(a)
OD550nm of supernate (a.u)
Number of separation steps
MC@RhB-1
MCR400
MC@RhB-2
(b)
O.D (a.u)
Wavelength (nm)
MCR400
MC@RhB-1
MC
Rhodamine B
MC@RhB-2
(O.D/1.6)
(c)
Fluorescence (a.u)
Wavelength (nm)
MCR400
Rhodamine B
MC@RhB-1
MC@RhB-2

Figure 2

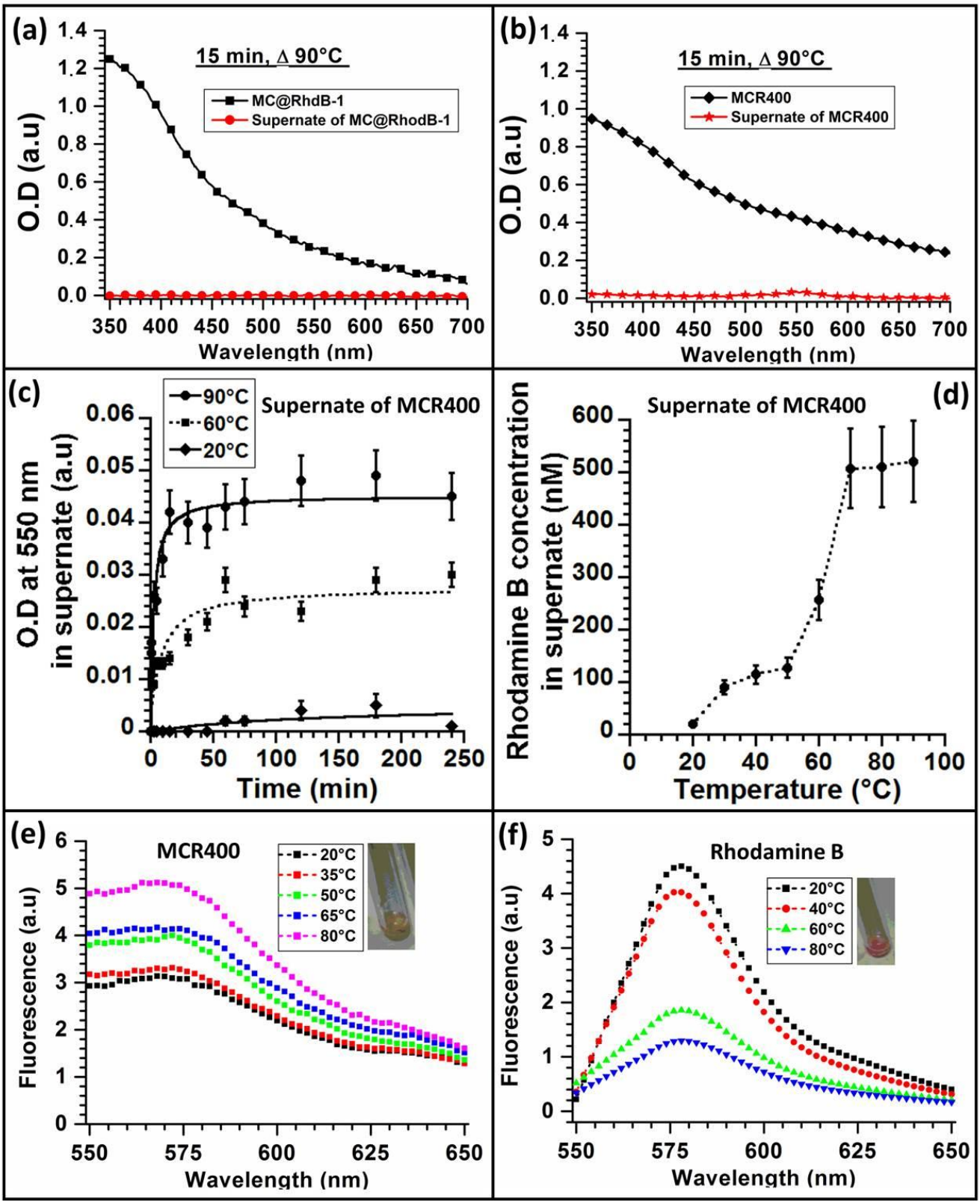
(a)
15 min, Δ 90°C
MC@RhdB-1
Supernate of MC@RhodB-1
O.D (a.u)
Wavelength (nm)
(b)
15 min, Δ 90°C
MCR400
Supernate of MCR400
O.D (a.u)
Wavelength (nm)
(c)
90°C
60°C
20°C
Supernate of MCR400
O.D at 550 nm in supernate (a.u)
Time (min)
(d)
Supernate of MCR400
Rhodamine B concentration in supernate (nM)
Temperature (°C)
(e)
MCR400
20°C
35°C
50°C
65°C
80°C
Fluorescence (a.u)
Wavelength (nm)
(f)
Rhodamine B
20°C
40°C
60°C
80°C
Fluorescence (a.u)
Wavelength (nm)

Figure 3

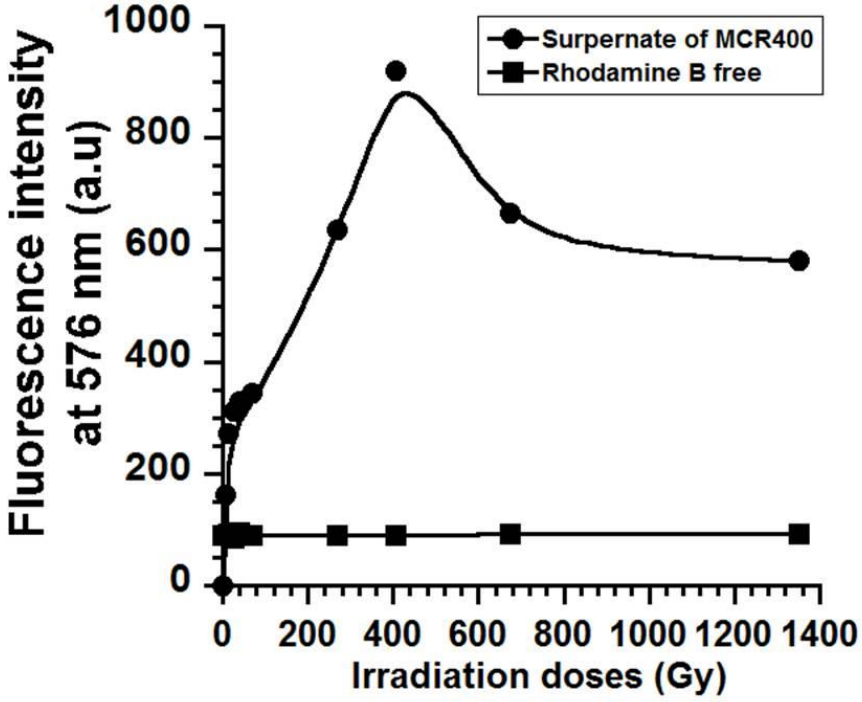
Surpernate of MCR400
Rhodamine B free
Fluorescence intensity at 576 nm (a.u)
1000
800
600
400
200
0
0
200
400
600
800
1000
1200
1400
Irradiation doses (Gy)

Figure 4

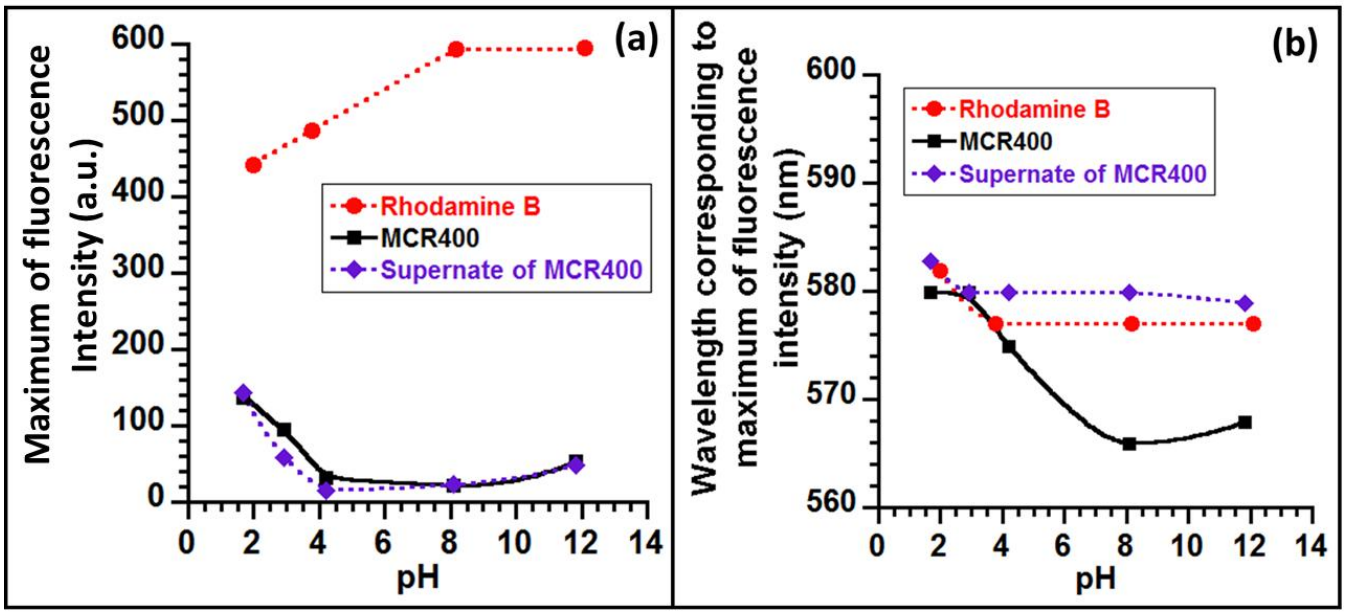
(a)
Maximum of fluorescence Intensity (a.u.)
600
500
400
300
200
100
0
0
2
4
6
8
10
12
14
pH
Rhodamine B
MCR400
Supernate of MCR400
(b)
Wavelength corresponding to maximum of fluorescence intensity (nm)
600
590
580
570
560
0
2
4
6
8
10
12
14
pH
Rhodamine B
MCR400
Supernate of MCR400

Figure 5

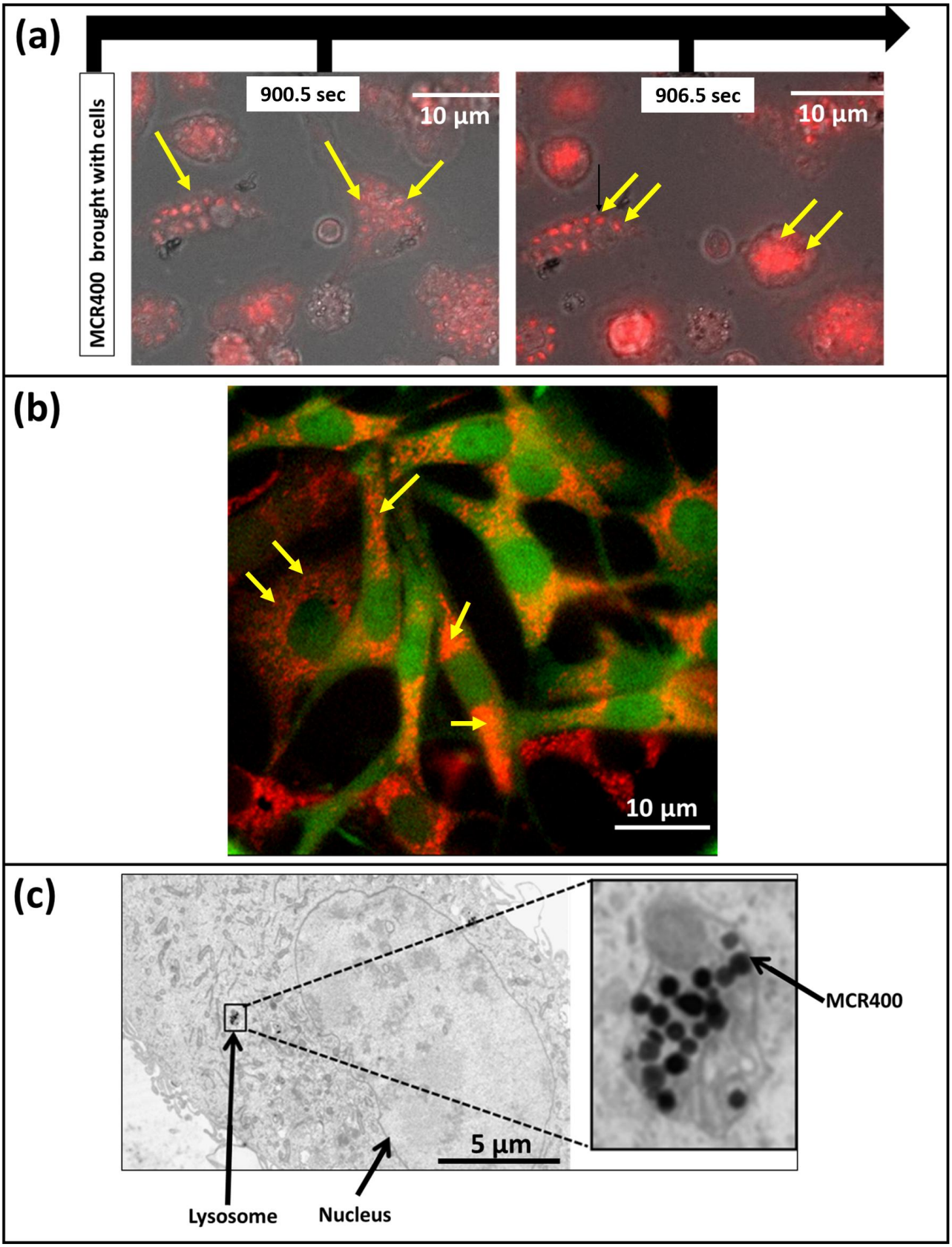
(a)
MCR400 brought with cells
900.5 sec
10 µm
906.5 sec
10 µm
(b)
10 µm
(c)
MCR400
5 µm
Lysosome
Nucleus

Figure 6

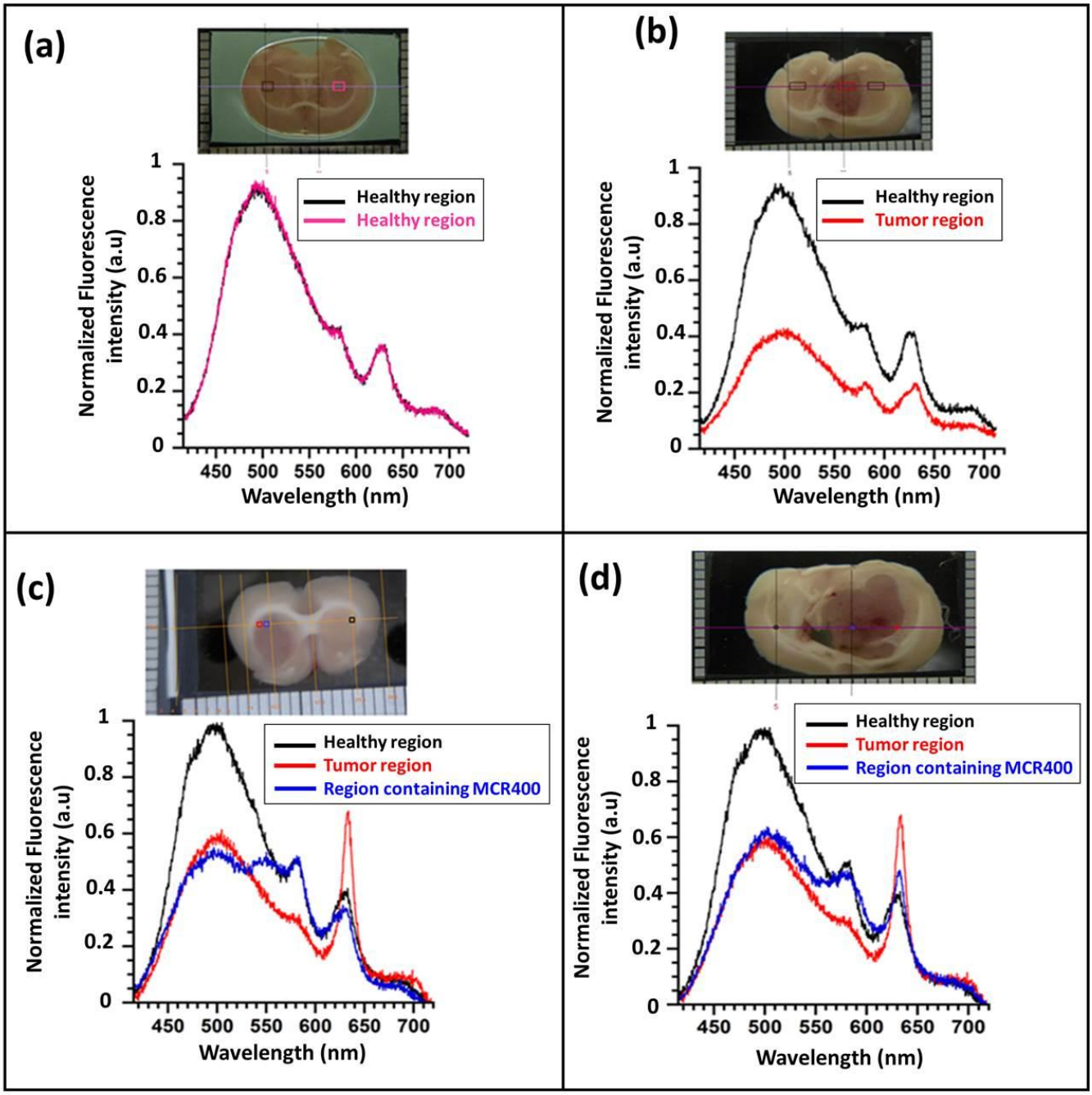
(a)
Normalized Fluorescence intensity (a.u)
Wavelength (nm)
Healthy region
Healthy region
(b)
Normalized Fluorescence intensity (a.u)
Wavelength (nm)
Healthy region
Tumor region
(c)
Normalized Fluorescence intensity (a.u)
Wavelength (nm)
Healthy region
Tumor region
Region containing MCR400
(d)
Normalized Fluorescence intensity (a.u)
Wavelength (nm)
Healthy region
Tumor region
Region containing MCR400

Figure 7